A deterministic method study of the impact of the Pauli principle in double-gate MOSFETs

Zhao Kai(赵 凯)[a)b)†], Christoph Jungemann[b)], and Liu Xiao-Yan(刘晓彦)[a)]

[a)] *Institute of Microelectronics, Peking University, Beijing* 100871, *China*

[b)] *Chair of Electromagnetic Theory, RWTH Aachen University, D*-52056 *Aachen, Germany*

(Received 11 April 2012; revised manuscript received 3 May 2012)

The Pauli principle is included in a multisubband deterministic solver for two-dimensional devices without approximations. The nonlinear Boltzmann equations are treated properly without compromising on accuracy, convergence, or CPU time. The simulation results indicate the significant impact of the Pauli principle on the transport properties of the quasi-2D electron gas, especially for the on state.

Keywords: Pauli principle, two-dimensional MOSFET, degeneracy, Fourier harmonics expansion

PACS: 85.30.De **DOI:** 10.1088/1674-1056/21/11/118501

1. Introduction

It is well-known that electrons cannot occupy the same quantum state simultaneously, which is the Pauli principle. In the case of MOSFETs, the impact of the Pauli principle in the inversion channel is more significant than that in the bulk silicon due to the lower density of states (DOS) and that the electrons are pushed toward higher energies. Therefore, including the Pauli principle in the simulation of a quasi-two-dimensional electron gas is of great importance.

The inclusion of the Pauli principle in the Monte Carlo (MC) method was implemented by Lugli and Ferry[1] by introducing a rejection technique,[2] which utilized the presence of an evolving MC distribution. This treatment entails an ensemble simulation with many particles in order to resolve the distribution function in the phase space, which makes its application in devices almost impossible due to the intensive computational resources required. Different approximations have been reported to reduce the CPU time.[3−5] However, their accuracies are doubtful.[6]

The deterministic Boltzmann solver provides such a complete distribution function that it does not inherently suffer from that difficulty.[7] Simulations including the Pauli principle based on a spherical harmonics expansion (SHE) method[8] for both bulk systems[6] and two-dimensional (2D) devices[9] have been reported. However, the impact of the Pauli principle was not obvious in those cases, since the quantum confinement effect was not considered, and a much larger three-dimensional DOS was employed. An intrinsic 2D deterministic Boltzmann solver based on the Fourier harmonics expansion (FHE) method has been proposed for quasi-2D hole gas simulations.[10,11] In this paper, the impact of the Pauli principle for a 16 nm double gate nMOSFET is numerically investigated using an electron FHE solver.

2. Approach

The probability of a state $\boldsymbol{k}$ to accept a transmitted electron from an initial state $\boldsymbol{k}'$ is in general proportional to the probability $[1-f(\boldsymbol{k})]$ known as the Pauli factor, which results in a nonlinear scattering integral. In the usual MC device simulations, this factor is approximated by a Fermi–Dirac distribution without including the displacement of the distribution in the phase space. This approximation neglects an important part of the response of the scattering integral to the displacement of the distribution, and results in a questionable mobility.[12] To avoid these disadvantages, the Boltzmann transport equation (BTE) is handled deterministically by expanding into a set of Fourier harmonics $\mathrm{Y}_m(\varphi)$[13] in the following way:

$$\frac{1}{(2\pi)^2}\int \{\mathrm{BTE}\}\,\delta\left(\varepsilon_{\parallel}-\varepsilon_{\parallel}\left(y,\boldsymbol{k}^*\right)\right)\mathrm{Y}_m(\varphi)\mathrm{d}^2k^*, \quad (1)$$

where $\boldsymbol{k}^*$ is the Herring–Vogt[14] transformed wave vector, and $\varepsilon_{\parallel}\left(y,\boldsymbol{k}^*\right)$ is the subband kinetic energy.

†Corresponding author. E-mail: k.zhao.chn@gmail.com

© 2012 Chinese Physical Society and IOP Publishing Ltd

The resultant stationary balance equation for the i-th subband in the ν-th valley reads

$$\sum_{m'=0}^{M}\left\{L_{m,m'}\left[g_{m'}^{i,\nu}\left(y,\varepsilon_{\parallel}\right)\right]-W_m\left[g_m^{i,\nu}\left(y,\varepsilon_{\parallel}\right)\right]\right\}=0, \tag{2}$$

where m and m' are the Fourier harmonics orders, M is the maximum expansion order, $L_{m,m'}$ is the free-streaming operator,[13] W_m is the scattering operator, y is the position of transport direction (Fig. 1), and $g_m^{i,\nu}$ is the energy distribution function expanded with the Fourier harmonics, which is the product of the 2D $\boldsymbol{k}$-space density of states Z and the expanded distribution function $f_m^{i,\nu}$. Only phonon and surface roughness scatterings whose transition rate c_η is independent of the scattering angle are considered in this work. However, its extension to a general case is straightforward (by expanding c_η onto a different set of Fourier harmonics). The scattering integral W_m can be decomposed into the in-scattering part $W_m^{\rm in}$ and the out-scattering part $W_m^{\rm out}$. Let η denote the scattering mechanism index with an energy transfer $\hbar\omega_\eta$, the in-scattering integral yields

$$\begin{aligned}W_m^{\rm in}=&\sqrt{2\pi}\sum_{i'\nu',\eta,\mp}c_{\eta,\mp}^{i,\nu,i',\nu'}\left(y,\varepsilon_{\parallel}\pm\hbar\omega_\eta\right)\\&\times\left(Z_m^{i,\nu}\delta_{m,0}-g_m^{i,\nu}\left(y,\varepsilon_{\parallel}\right)\right)\\&\times g_0^{i',\nu'}\left(y,\varepsilon_{\parallel}\pm\hbar\omega_\eta\right),\end{aligned} \tag{3}$$

where $c_{\eta,\mp}^{i,\nu,i',\nu'}$ is the transition rate from the initial state with kinetic energy $\varepsilon'_{\parallel}=\varepsilon_{\parallel}\pm\hbar\omega_\eta$ to the final state $\varepsilon_{\parallel}$. For an elastic scattering mechanism η, $\hbar\omega_\eta=0$, $c_{\eta,+}=c_\eta$, and $c_{\eta,-}=0$. The $Z_m^{i,\nu}$ is the expanded density of states of the i-th subband in the ν-th valley. If a parabolic band structure is adopted, $Z^{i,\nu}$ becomes isotropic and equals $Z_0^{i,\nu}\mathrm{Y}_0\left(\varphi\right)$. In contrast to the 3D $\boldsymbol{k}$-space DOS which is proportional to the square root of energy, $Z^{i,\nu}$ is a constant within a subband.

Analogously, the out-scattering integral is given by

$$\begin{aligned}W_m^{\rm out}=&\sqrt{2\pi}\sum_{i'\nu',\eta,\mp}c_{\eta,\mp}^{i',\nu',i,\nu}\left(y,\varepsilon_{\parallel}\right)g_m^{i,\nu}\left(y,\varepsilon_{\parallel}\right)\\&\times\left(Z_0^{i',\nu'}-g_0^{i',\nu'}(y,\varepsilon_{\parallel}\pm\hbar\omega_\eta)\right).\end{aligned} \tag{4}$$

It is worth noting that a nonlinear term in the form of a double product of energy distribution functions $g_m\,g_0$ is introduced by the Pauli principle. To solve this nonlinear BTE, a Newton–Raphson scheme is adopted analogously to the SHE case.[15]

3. Results

The impact of the Pauli principle is investigated for a 16 nm double gate MOSFET (Fig. 1). The doping concentrations in the source and the drain are up to the order of 10^{20} cm^{-3}. The thickness of the silicon layer is 5 nm. A one-dimensional Schrödinger equation is solved to capture the quantum confinement effect in the x direction. All the results are simulated using a parabolic band structure, whereas a full band expansion is also possible.[16]

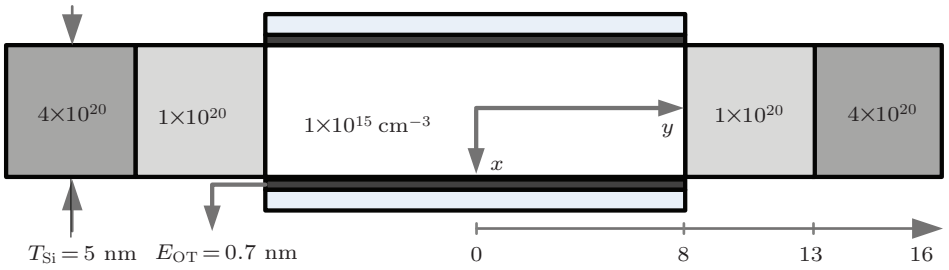


Fig. 1. Structure and doping profile of the simulated double gate MOSFET.

The convergence behavior with and without the Pauli principle under different bias conditions is demonstrated in Fig. 2. An initial guess of the electrostatic potential is obtained using the drift diffusion (DD) model, and then improved by solving the Schrödinger and the Poisson equations iteratively. As the procedure is iterated, a steady electrostatic potential will eventually be obtained, which is already good enough for small bias cases. After this, a coupled scheme for the Boltzmann, Schrödinger, and Poisson equations is used. The iteration count in Fig. 2 is for the coupled scheme. If the Pauli principle is included,

a Newton–Raphson scheme, whose convergence behavior is shown in Fig. 3, is employed in each coupled iteration to solve the nonlinear BTE. The tolerance of the Newton–Raphson scheme is set to 10^{-14} with respect to the norm of the residue. Three or four steps are sufficient to obtain a converged solution of the nonlinear equations. If a large bias is applied, iterations with the Pauli principle converge a little faster than that without. However, the opposite trend is found for small bias cases. It is interesting to note that for the MC simulations, large bias cases always converge slower than small bias cases.

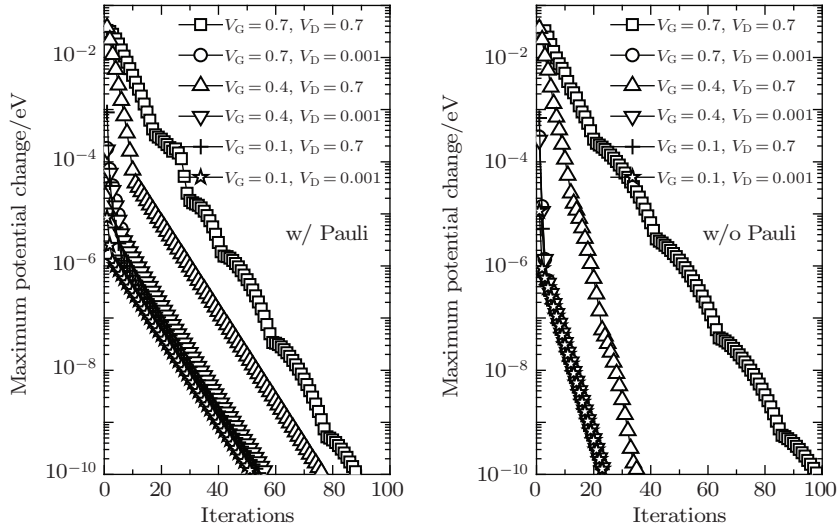


Fig. 2. Convergence behaviors (a) with and (b) without the Pauli principle. The V_G and V_D are the gate the drain voltages, respectively, and they are given in units of V.

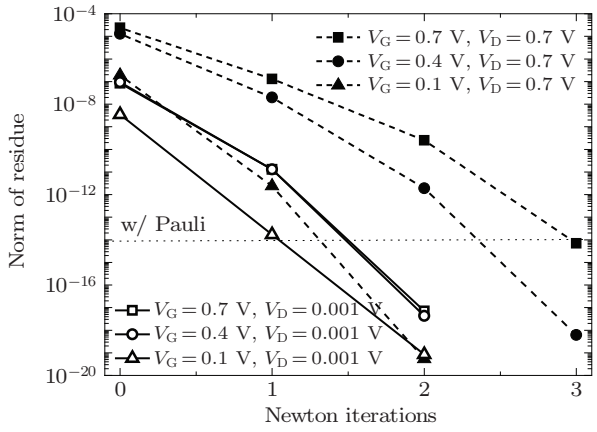


Fig. 3. Convergence behaviors of the Newton–Raphson iterations.

In Fig. 4, the zeroth order expansions of the distribution function g_0, which correspond to the electron distribution in the energy space, are compared at different positions along the transport direction. Figures 4(a) and 4(b), in which the Pauli principle is considered, show the lowest $10k_BT$ energy regions for on-state ($V_G = 0.7$ V) and subthreshold ($V_G = 0.2$ V), respectively. As a consequence of the reduced occupancy of each allowed state, the electrons are pushed into higher energy levels, and the degeneracy effect is clearly visible at -8 nm and 13 nm for both cases. At the middle of the channel (0 nm), the electrons with low energy are heavily scattered, and the periodic step-like structures appear. At the drain end of the channel (8 nm), the step structures disappear because the injection from the drain reinforces the distribution in the low energy region. Contrary to Figs. 4(a) and 4(b), non-degeneracy and typical Boltzmann statistics are clearly shown as they should be in Figs. 4(c) and 4(d) without the Pauli principle. In Figs. 4(a) and 4(c), a prominent increase arises in the low kinetic energy region at the source end of the channel (-8 nm) no matter whether the Pauli principle is considered or not. This is because the electrons injected from the source with insufficient energy to overcome the barrier to the channel are reflected and accumulated in the front of the virtual source.[17] Since direct tunneling is not considered in this work, these accumulated electrons in the low energy region can only cross the virtual source if assisted by scattering events.

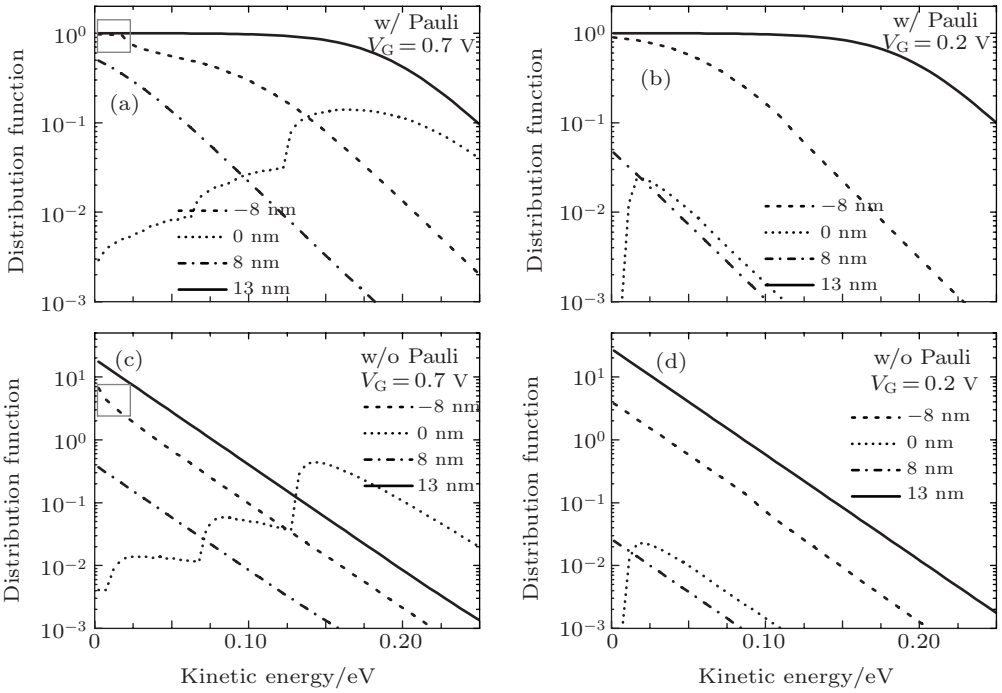


Fig. 4. Electron distribution functions ((a), (b)) with and ((c), (d)) without the Pauli principle in the lowest $10k_BT$ energy region for $V_D = 0.7$ V.

The on-state electron densities and the lowest subband energy with or without the Pauli principle are shown in Fig. 5. The continuous curves refer to the case including the Pauli principle, and the starred curves indicate the results without the Pauli principle. As expected, the impact of the Pauli principle on the density is neglectable except at the places with large electric fields. However, its impact on the subband energy is significant, especially in the strong degenerate regions. If the quasi-Fermi level stays the same in these regions, the subbands must be lowered in the cases with the Pauli principle to achieve the same electron sheet density as that in the cases without the Pauli principle.

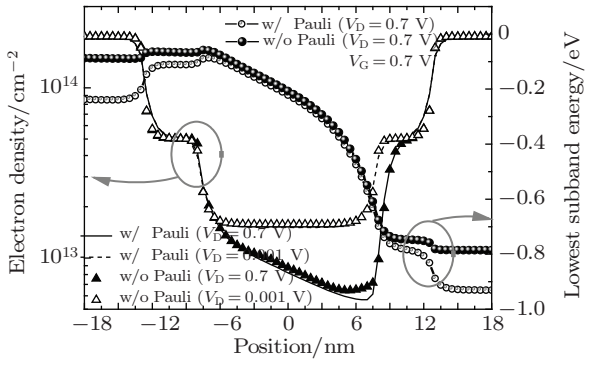


Fig. 5. Electron density and the lowest subband energy along the transport direction.

Figure 6 shows the net and directional currents along the channel at $V_G = 0.7$ V and $V_D = 0.7$ V. The forward current considering the Pauli principle is larger than that neglecting the Pauli principle in the non-degenerate region of the channel, whereas it is much smaller in the source and the drain. In the meantime, the backward current has a very close value in the channel, except in the k_BT layer.[17] However, it is important to note that only the backward current at the virtual source is determinant, where it is 2.68 times larger in the case with the Pauli principle than that without. The net currents with and without the Pauli principle are 3313 A/m and 3905 A/m, respectively, which are in full compliance with the directional currents. In addition, the exact net current continuity is ensured by the adoption of the box-integration method.

In Fig. 7 the net and the directional electron velocities with and without the Pauli principle are compared under the same conditions as those in Fig. 6. The net velocity without the Pauli principle increases more rapidly in the first half of the channel, and then synchronously with that in the case including the Pauli principle. However, if the Pauli principle is neglected, the directional velocities are much larger, especially the backward-moving velocity. The triangle-like peaks of the backward-moving velocity at the drain end of the channel for both cases are due to the injections from the drain reservoir, but they

both vanish quickly because of the strong driving force pointing in the opposite direction.

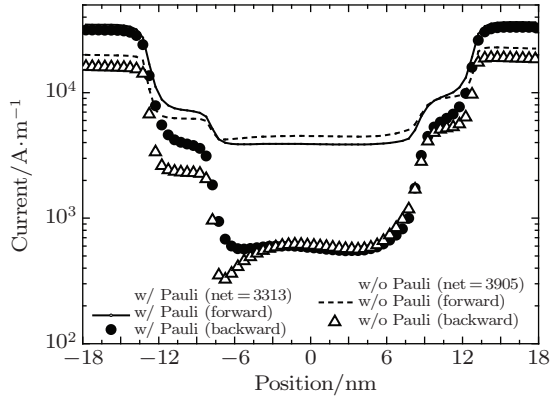


Fig. 6. Directional current along the transport direction at $V_G = 0.7$ V and $V_D = 0.7$ V.

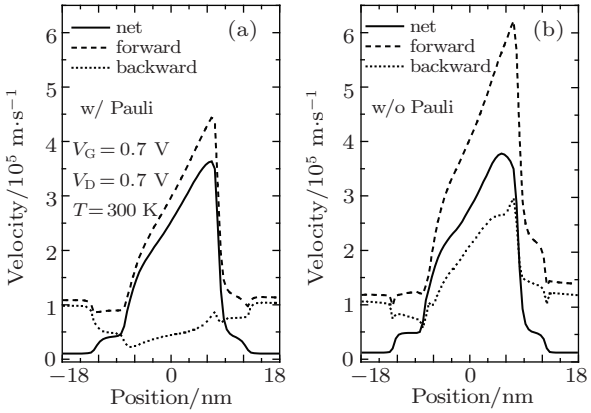


Fig. 7. Net, forward, and backward electron velocities along the channel at the on state (a) with and (b) without the Pauli priciple.

The output characteristics at room temperature are presented in Fig. 8, which clearly shows that the impact of the Pauli principle is critical. The overestimation of the drain current by neglecting the Pauli principle may reach 18% for the on state, but is neglectable in the subthreshold region.

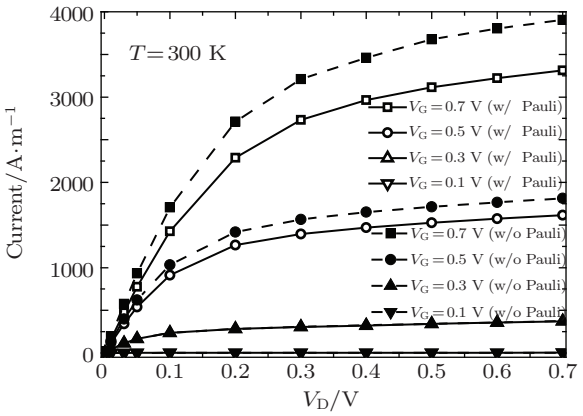


Fig. 8. Output characteristics with and without the Pauli principle.

4. Conclusion

The inclusion of the Pauli principle in a stable deterministic Boltzmann solver based on the FHE method is presented in this paper, and its impact for 2D double gate nMOSFETs is investigated with consideration of the quantum confinement effect for the first time. The nonlinear equations are properly treated by introducing a Newton–Raphson iteration without suffering from convergence degradation. This solver reaches real applicability in strong degenerate simulations in contrast to the MC approach. The Pauli principle plays an important role in quasi-2D electron gas transport because the degeneracy is essential, especially for the on state. The neglection of the Pauli principle will overestimate the current and the electron velocity, and will provide overly optimistic results.

Acknowledgment

The first author gratefully acknowledges DAAD (Deutscher Akademischer Austausch Dienst) for the support during his stay in Germany and Dr. Hong Sung-Min for helpful discussion on the deterministic Boltzmann solver.

References

[1] Lugli P and Ferry D 1985 *IEEE Trans. Electr. Dev.* **32** 2431
[2] Jacoboni C and Reggiani L 1983 *Rev. Mod. Phys.* **55** 645
[3] Fischetti M V and Laux S E 1988 *Phys. Rev.* B **38** 9721
[4] Pantoja J M M and Franco J L S 1997 *IEEE Electron Dev. Lett.* **18** 258
[5] Mateos J, González T, Pardo D, Hoël V, Happy H and Cappy A 2000 *IEEE Trans. Electr. Dev.* **47** 250
[6] Jungemann C 2007 *Proc. SPIE* **6600** 660007
[7] Piazza A J, Korman C E and Jaradeh A M 1999 *IEEE Trans. Computer-Aided Des.* **18** 1730
[8] Gnudi A, Ventura D, Baccarani G and Odeh F 1993 *Sol. St. Electr.* **36** 575
[9] Hong S M and Jungemann C 2010 *J. Comput. Elect.* **9** 153
[10] Pham A, Jungemann C and Meinerzhagen B 2008 *Proc. IEDM* 115
[11] Pham A, Jungemann C and Meinerzhagen B 2009 *J. Comput. Elect.* **8** 242
[12] Ungersböck E and Kosina H 2005 *Proc. SISPAD* 311
[13] Zhao K, Hong S M, Jungemann C and Han R Q 2010 *Proc. SISPAD* 17-A.2
[14] Herring C and Vogt E 1956 *Phys. Rev.* **101** 944
[15] Hong S M and Jungemann C 2009 *J. Comput. Elect.* **8** 225
[16] Matz G, Hong S M and Jungemann C 2010 *Proc. SISPAD* 09-B.3
[17] Lundstrom M and Ren Z 2002 *IEEE Trans. Electr. Dev.* **49** 133